Resonant stimulated Brillouin scattering of orthoexcitons in Cu_2O

Christian Sandfort,* Jan Brandt, Dietmar Fröhlich, Giorgio Baldassarri Höger von Högersthal, and Manfred Bayer
Fakultät Physik, Technische Universität Dortmund, D-44221 Dortmund, Germany

Heinrich Stolz
Institut für Physik, Universität Rostock, D-18501 Rostock, Germany
(Received 20 May 2009; published 4 December 2009)

Resonant excitation of 1*S* orthoexcitons in Cu_2O in a magnetic field leads to a fine structure in the Γ_3^- and Γ_5^- optical phonon assisted emission. This fine structure can be attributed to intraband and interband resonant Brillouin scattering. For increasing power a strong nonlinear enhancement of the intensity of this fine structure and a splitting due to preferential scattering into forward/backward direction is observed, indicating a stimulation of the scattering processes. We present a detailed analysis of the kinematics of the transversal/longitudinal acoustic (TA/LA) phonon scattering processes. The exclusive observation of slow TA interband scattering and LA intraband scattering is deduced from selection rules for acoustic phonon scattering and the deformation potentials. Furthermore, a strong asymmetric resonance dependence is observed.

DOI: 10.1103/PhysRevB.80.245201 PACS number(s): 78.35.+c, 71.35.Lk, 78.20.Hp, 78.40.Fy

I. INTRODUCTION

As was first shown for GaAs,[1] Brillouin scattering between exciton polaritons can be observed directly. Later Brillouin scattering was observed in CdS via the additional emission of an optical phonon.[2] The observation of acoustic phonon scattering by two-phonon processes [longitudinal/transversal acoustic (LA/TA) and longitudinal optical (LO)] has at least two advantages: first, the additional energy shift by emission of an optical phonon makes it easy to suppress scattered laser light. Second, the dispersionless LO phonon allows the observation of final states of k values, whose probability for emission of photons tends to zero, because the photon contribution of the final polariton state tends to zero. In Cu_2O Brillouin scattering from the 1*S* excitons can only be observed by a two-phonon process, since the final state has even parity and thus can only be detected by the additional emission of an optical phonon of odd parity.[3]

In Cu_2O inelastic scattering of photons with optical phonons (Raman scattering) was studied intensively in the past.[4,5] It has already been shown that LA and TA phonon scattering (Brillouin scattering) has to be taken into account to analyze the rich spectrum of intraband and interband scattering within the orthoexciton subbands.[3] These Brillouin scattering processes can be stimulated for sufficiently high light intensities, connected with a pronounced line narrowing compared to the spontaneous scattering.

The yellow 1*S*-excitons in Cu_2O consist of the three-fold quadrupole allowed orthoexciton of Γ_5^+ symmetry split of by 12.12 meV (Ref. 6) to higher energy from the optically forbidden paraexciton of Γ_2^+ symmetry by isotropic exchange. In a magnetic field, the orthoexciton splits into the three states $M=0$, $M=\pm 1$,[3] whose energetic separation is determined by the magnetic field strength. k^2-dependent exchange interaction yields anisotropic masses for the three orthoexciton states.[7] Exciting the highest state $M=+1$ resonantly at $\mathbf{k}_0$ leads to intraband and interband scattering with LA and TA phonons to the lower lying $M=0$ and $M=-1$ orthoexcitons. A weak spontaneously scattered occupation is the source for stimulated Brillouin scattering between the orthoexciton states. With a detailed analysis of the kinematics we show that these scattering processes strongly depend on the applied magnetic field. Besides the prerequisite of energy and momentum conservation, the possibility for stimulated Brillouin scattering is additionally governed by selection rules and deformation potentials leading to a pronounced $\mathbf{k}$ dependence. The analysis reveals the possibility to excite a state in the lowest orthoexciton subband with arbitrary k and in particular with $k=0$ for three distinct field strengths. A strong asymmetric resonance dependence within a few μeV increases the relevant parameter space even more.

II. THEORY

Sound velocities in Cu_2O depend on $\mathbf{k}$ direction, i.e., the TA phonon is degenerate along $\mathbf{k}\|[001]$ and splits into a slow TA (STA) phonon and a fast TA (FTA) phonon along $[1\bar{1}0]$. Possible interband and intraband scattering along $\mathbf{k}\|[1\bar{1}0]$ with STA and LA phonons within the orthoexciton subbands for excitation of the $M=+1$ orthoexciton is illustrated in Fig. 1 for a field strength of 4 T in Voigt configuration. The red solid lines (TA phonon sound velocity $v_{STA}=1.14\cdot 10^3$ ms^{-1}) represent forward and backward scattering of the STA phonon, the blue solid lines (LA phonon sound velocity $v_{LA}=4.60\cdot 10^3$ ms^{-1}) forward and backward scattering of the LA phonon along $\mathbf{k}\|[1\bar{1}0]$. The sound velocities have been determined from the kinematical analysis (Fig. 2) and agree well with data in the literature.[8–10]

Selection rules for these intraband and interband scattering processes can be derived from the acoustic phonon interaction Hamiltonian, which in Cu_2O contains four terms H_1, H_3, H_4 and H_5 of Γ_1^+, Γ_3^+, Γ_4^+, and Γ_5^+ symmetry, respectively.[11]

For STA phonons along $\mathbf{k}\|[1\bar{1}0]$, only $H_3\neq 0$ and $H_4\neq 0$, whereas for FTA phonons, only $H_4\neq 0$ and $H_5\neq 0$. Calculation of the matrix elements $|\langle O_F|H_i|O_I\rangle|^2$ leads to selection rules for the acoustic phonons with the excited orthoex-

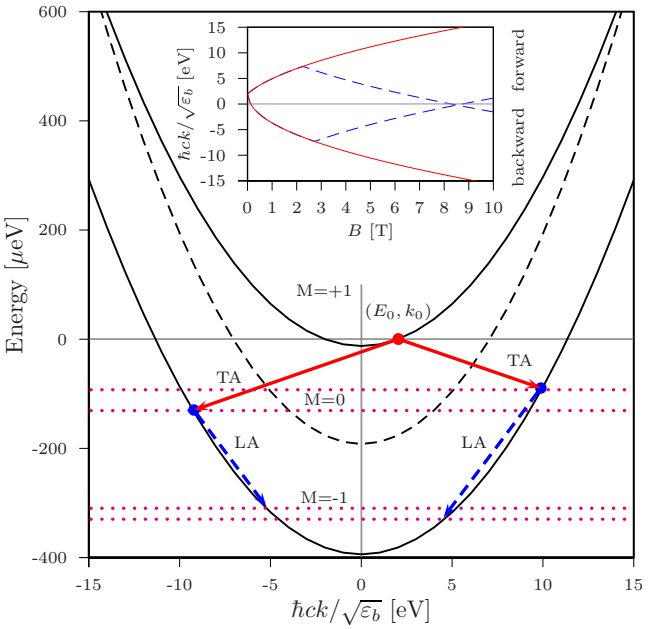

FIG. 1. (Color online) Intraband and interband Brillouin scattering within the orthoexciton parabolas for $\mathbf{k}\|[1\bar{1}0]$ and $B=4$ T in Voigt configuration: upper parabola, $M=+1$ dispersion; dashed parabola, $M=0$ dispersion; lower parabola, $M=-1$ dispersion; solid red arrows, interband scattering with STA phonons; dashed blue arrows, intraband scattering with LA phonons; $E=0$ μeV corresponds to the resonance of the $M=+1$ orthoexciton, wavenumber $x=\hbar ck/\sqrt{\varepsilon_b}$ with $\varepsilon_b=8.64$. The magenta dotted lines indicate the measured energy of the Brillouin scattering lines. Inset: calculated wavenumber dependence of the scattering on the magnetic field; red solid lines, STA phonon interband scattering ($M=+1$ to $M=-1$); and blue dashed lines, LA intraband scattering within $M=-1$.

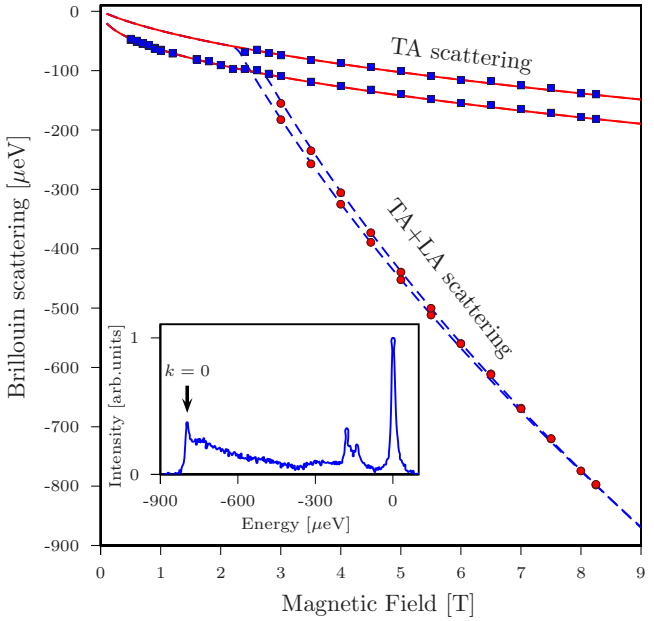

FIG. 2. (Color online) Energetic positions of Brillouin scattering lines. $E=0$ μeV corresponds to the Raman transiton; red solid lines, TA scattering; blue dashed lines, TA+LA scattering; and blue squares, measured TA scattering; read dots, measured TA+LA scattering. Inset: Γ_5^- phonon assisted emission at 8.25 T. Arrow marks TA+LA scattering to $k=0$ within the $M=-1$ subband.

citon state $|O_I\rangle$ (here $M=+1$) and the final orthoexciton state $|O_F\rangle$ ($M=0,-1$). They show that for STA phonons scattering is allowed only from $M=+1$ to the $M=-1$, whereas for the FTA phonons only scattering to the $M=0$ state is possible. Comparing the scattering probabilities calculated from H_3 and H_5 shows that the probability for TA phonons with Γ_3^+ symmetry is by an order of magnitude higher than for TA phonons with Γ_5^+ symmetry.[12] Therefore we consider only STA phonon scattering from $M=+1$ to $M=-1$ as sketched in Fig. 1.

In contrast to TA phonons, LA phonon scattering is the dominating scattering process for intraband scattering due to a large Γ_1^+ contribution to the scattering probability. Intraband scattering of LA phonons within the $M=-1$ orthoexciton starting from a state to which the TA phonon scatters from $M=+1$, is shown in Fig. 1. For the different scattering processes the dependence of the final wavevector on the magnetic-field strength is shown as an inset.

An overview of the selection rules for $\mathbf{k}\|[1\bar{1}0]$ in Voigt and Faraday configuration is shown in Table I. The relevant symmetry contributions of the Hamiltonian and the corresponding matrix elements $|\langle O_F|H_i|O_I\rangle|$ are listed for LA, STA and FTA Brillouin scattering. Note that the selection rules depend also on the wavevector $\mathbf{k}$ which is not shown here.

III. SETUP

In our experiments we use a single-frequency dye laser with a linewidth of about 5 neV to excite the orthoexciton resonantly at $(E_0,\mathbf{k}_0)$. The x-ray oriented sample is immersed in superfluid ^{4}He ($T\approx 1.4$ K) in a split coil cryostat, which allows the application of magnetic fields up to $B=10$ T in Faraday ($\mathbf{k}\|\mathbf{B}$) and Voigt configuration ($\mathbf{k}\perp\mathbf{B}$). The phonon assisted emission via Γ_5^- and Γ_3^- optical phonons is monitored by a camera behind a double monochromator with a resolution of 10 μeV.[13] The additional shift of the Brillouin resonances due to the optical phonons (10.58 meV for Γ_5^- phonons, 13.45 meV for Γ_3^- phonons) and the use of optical low pass filters allows an excellent supression of scattered laser light.

IV. RESULTS AND DISCUSSION

Figures 3 and 4 show the Γ_3^- and Γ_5^- phonon assisted emission of the orthoexciton, respectively. The zero point of the energy scale is shifted to the Stokes-Raman transition of the corresponding optical phonon. Additionally to the Raman peak at $E=0$ μeV, one observes Stokes and anti-Stokes lines due to interband and intraband Brillouin scattering. The anti-Stokes lines around 150 μeV and 510 μeV (marked by arrows in Fig. 3) can be attributed to TA phonon interband scattering and LA phonon intraband scattering, respectively. These lines show a very weak dependence on excitation intensity. On the Stokes-side of the spectrum one observes for low excitation intensities two Brillouin lines besides the Raman line. With increasing excitation intensity the emission

TABLE I. Selection rules for Brillouin scattering within $M=0,\pm1$ orthoexciton for $\mathbf{k}\|[1\bar{1}0]$ in Faraday ($B\|[1\bar{1}0]$) and Voigt-configuration ($B\|[001]$). The relevant symmetry contributions of the Hamiltonian and the corresponding matrix elements $|\langle O_F|H_i|O_I\rangle|$ are listed for LA, STA, and FTA Brillouin scattering as numbers in parenthesis; (-) means not allowed, zero matrix element.

	Faraday			Voigt		
	$M=-1$	$M=0$	$M=+1$	$M=-1$	$M=0$	$M=+1$
$M=-1$	LA ($\Gamma_1^+;\Gamma_3^+;\Gamma_5^+$)	LA	LA ($\Gamma_3^+;\Gamma_5^+$)	LA ($\Gamma_1^+;\Gamma_3^+$)	LA	LA (Γ_5^+)
	(1.68; 0.07; 0.08)	(-)	(0.22; 0.08)	(1.68; 0.15)	(-)	(0.16)
	STA	STA ($\Gamma_3^+;\Gamma_4^+$)	STA	STA (Γ_4^+)	STA	STA (Γ_3^+)
	(-)	(0.31; 0.01)	(-)	(0.02)	(-)	(0.44)
	FTA	FTA ($\Gamma_4^+;\Gamma_5^+$)	FTA	FTA	FTA ($\Gamma_4^+;\Gamma_5^+$)	FTA
	(-)	(0.01;0.11)	(-)	(-)	(0.01;0.11)	(-)
$M=0$	LA	LA ($\Gamma_1^+;\Gamma_3^+;\Gamma_5^+$)	LA	LA	LA ($\Gamma_1^+;\Gamma_3^+$)	LA
	(-)	(1.68;0.15;0.16)	(-)	(-)	(1.68;0.29)	(-)
	STA ($\Gamma_3^+\Gamma_4^+$)	STA	STA ($\Gamma_3^+;\Gamma_4^+$)	STA	STA	STA
	(0.31;0.01)	(-)	(0.31;0.01)	(-)	(-)	(-)
	FTA ($\Gamma_4^+;\Gamma_5^+$)	FTA	FTA ($\Gamma_4^+;\Gamma_5^+$)	FTA ($\Gamma_4^+;\Gamma_5^+$)	FTA	FTA ($\Gamma_4^+;\Gamma_5^+$)
	(0.01;0.11)	(-)	(0.01;0.11)	(0.01;0.11)	(-)	(0.01;0.11)
$M=+1$	LA ($\Gamma_3^+;\Gamma_3^+$)	LA	LA ($\Gamma_1^+;\Gamma_3^+;\Gamma_5^+$)	LA (Γ_5^+)	LA	LA ($\Gamma_1^+;\Gamma_3^+$)
	(0.22;0.08)	(-)	(1.68;0.07;0.08)	(0.16)	(-)	(1.68;0.15)
	STA	STA ($\Gamma_3^+;\Gamma_4^+$)	STA	STA (Γ_3^+)	STA	STA (Γ_4^+)
	(-)	(0.31;0.01)	(-)	(0.44)	(-)	(0.02)
	FTA	FTA ($\Gamma_4^+;\Gamma_5^+$)	FTA	FTA	FTA ($\Gamma_4^+;\Gamma_5^+$)	FTA
	(-)	(0.01;0.11)	(-)	(-)	(0.01;0.11)	(-)

intensity of these lines increases with respect to the Raman line. For high excitation intensities there is a strong nonlinear increase in intensity of these Brillouin lines and each of them splits into two narrow lines.

Due to the smaller width of the Γ_5^- optical phonon in emission ($\gamma_5=8$ μeV) as compared to the width of the Γ_3^- optical phonon ($\gamma_3=21$ meV) (Ref. 13) these scattering processes, particularly the splitting of the energetically lower lying scattering lines, are resolved more clearly in the Γ_5^- phonon assisted emission (note the different energy scales of Figs. 3 and 4).

The intensity dependence of the Brillouin scattering as shown in the insets in Figs. 3 and 4 shows a nonlinear increase in the Brillouin scattering peaks with excitation intensity indicating the stimulated character of the scattering processes. The stimulation starts at a threshold value of about 2 kW/cm^2 and saturates above 16 kW/cm^2. This threshold-like behavior and saturation for high excitation intensities are typical for stimulated Brillouin scattering.[14]

A kinematical analysis shows that the first line at $E_{STA}^+=-92.9$ μeV (Fig. 4) corresponds to forward, the second one at $E_{STA}^-=-131$ μeV to backward interband scattering along $\mathbf{k}\|[1\bar{1}0]$ with STA phonons between $M=+1$ and $M=-1$ orthoexcitons. The third and the fourth line at $E_{LA}^-=-310$ μeV and $E_{LA}^+=-330$ μeV can be identified as backward and forward intraband scattering of LA phonons within the $M=-1$ subband. The Γ_3^- data (Fig. 3) show the same results, as far as the fine structure can be resolved.

For low excitation intensities, Brillouin scattering takes place in $\mathbf{k}$ directions determined by energy and momentum

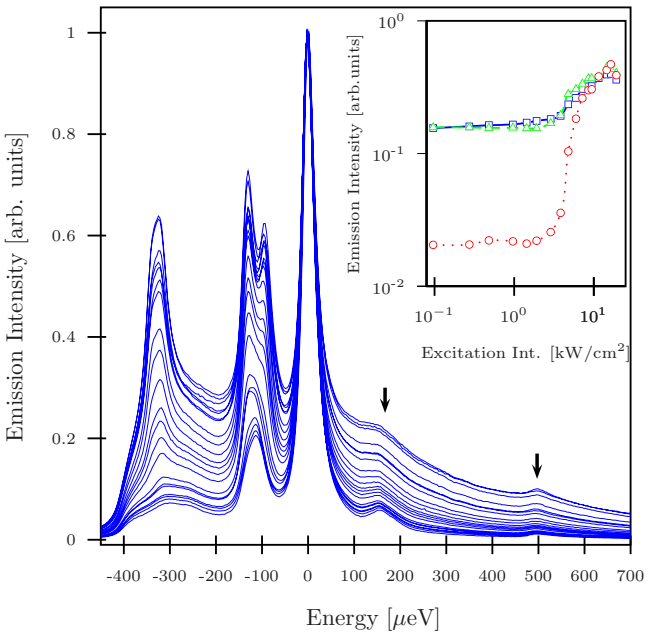

FIG. 3. (Color online) Γ_3^- phonon assisted emission of orthoexcitons for different excitation intensities ($B=4$ T in Voigt configuration). $E=0$ μeV corresponds to the resonance of the $M=+1$ orthoexciton shifted to lower energy by the energy of the Γ_3^- LO phonon (13.45 meV). Inset: dependence of emission intensity on laser intensity; blue squares, TA forward scattering; green triangles, TA backward scattering; red empty dots, TA+LA scattering. Arrows mark anti-Stokes Brillouin scattering of LA phonons.

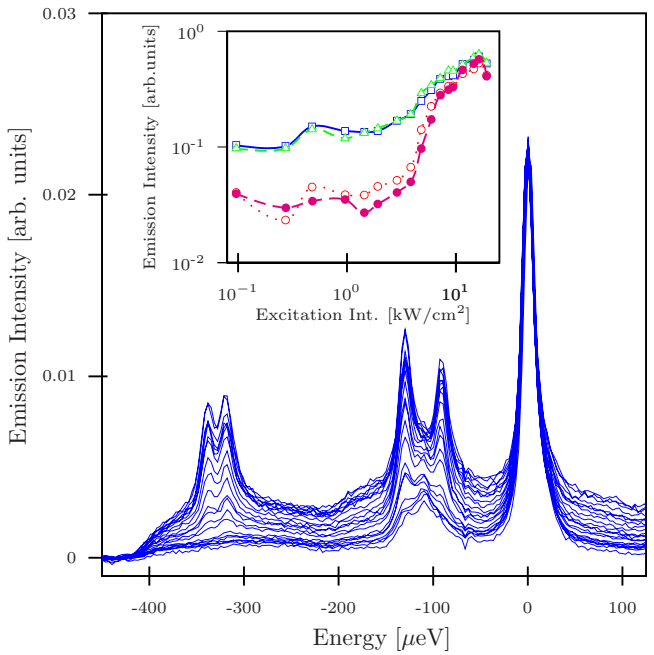

FIG. 4. (Color online) Γ_5^- phonon assisted emission of orthoexcitons for different excitation intensities ($B=4$ T in Voigt configuration). $E=0$ μeV corresponds to the resonance of the $M=+1$ orthoexciton shifted to lower energy by the energy of the Γ_5^- LO phonon (10.58 meV). (Ref. 8) Note: the range of the energy scale is reduced by a factor of two in comparison to the one in Fig. 3. Inset: dependence of emission intensity on laser intensity; blue squares, TA forward scattering; green triangles, TA backward scattering; red empty dots, TA+LA forward scattering; magenta solid dots, TA +LA backward scattering.

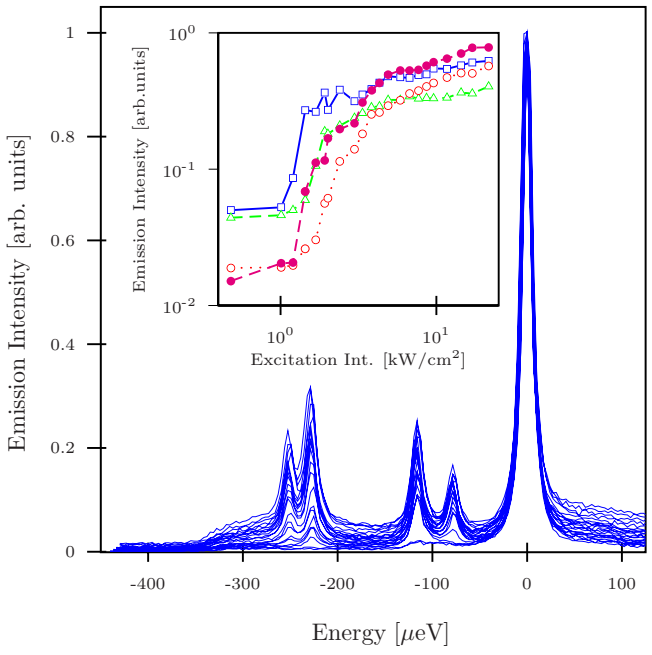

FIG. 5. (Color online) Γ_5^- phonon assisted emission of orthoexcitons for different excitation intensities ($B=6$ T in Faraday configuration). $E=0$ μeV corresponds to the resonance of the $M=0$ orthoexciton shifted to lower energy by the energy of the Γ_5^- LO phonon (10.58 meV). Inset: dependence of emission intensity on laser intensity; blue squares, TA forward scattering; green triangles, TA backward scattering; red empty dots, TA+LA forward scattering; magenta solid dots, TA+LA backward scattering.

conservation leading to a "plateau" from $E^+_{TA/LA}$ up to $E^-_{TA/LA}$ in the phonon assisted emission. As soon as the stimulation threshold is reached the "plateau" splits into two peaks which we attribute to forward and backward scattering. This can be understood in a simple picture considering two waves: one for the phonon and one for the exciton. As interference of two waves is maximized for parallel or antiparallel propagating waves, there is a preference for forward/backward stimulated scattering.[15] Since the LA phonon scattering processes do not simply copy the occupation generated by stimulated TA scattering but set in at higher excitation intensities, we conclude that the LA scattering process itself is stimulated with a slightly higher threshold. As the temperature of the exciton gas obtained from a fit of the spectra in Fig. 3 is approximately the bath temperature (<2 K), a possible increased occupation of acoustic phonons due to heating can be ruled out. Though an increased occupation of acoustic phonons leads to a higher intensity of the Brillouin scattering lines, it does not give rise to a preferential scattering into forward and backward direction as stimulated Brillouin scattering does.

The dotted lines in Fig. 1 represent the energetic positions $E^{+/-}_{STA}$ and $E^{+/-}_{LA}$ of the measured peaks which quantitatively match the interband and intraband scattering processes discussed before. The positions of the lines depend strongly on the magnetic field as shown in Fig. 2 since the splitting of the orthoexciton subbands increases linearly with magnetic field. The solid lines represent the calculated kinematics for STA interband scattering from $M=+1$ to $M=-1$, the dashed lines represent LA intraband scattering within the $M=-1$ orthoexciton. In Fig. 2 one recognizes a threshold for LA intraband scattering at 2.25 T.

With increasing field strength the stimulation gain decreases. The scattering processes at higher field strength involve acoustic phonons with higher energy, since the splitting of the orthoexciton subbands increases with magnetic field. These "high"-energy phonons, however, are only weakly occupied at low temperatures yielding a higher stimulation threshold.

As seen in the inset of Fig. 1 the kinematics allows final scattering states in the lowest exciton subband with arbitrary wavevector k which is achieved by simply tuning the magnetic field. For three distinct field strengths this final wavevector vanishes ($k=0$): (i) at $B\approx 8.25$ T and $B\approx 8.75$ T by two phonon (STA/LA) forward and backward scattering, respectively (inset Fig. 1), and (ii) at ≈ 0.1 T by a one-phonon process (STA-backward scattering) The inset in Fig. 2 shows an example of stimulated scattering at 8.25 T where the wavevector of the final scattering state vanishes.

Figure 5 shows stimulated Brillouin scattering for $\mathbf{k}\|[1\bar{1}0]$ in Faraday configuration at $B=6$ T. Although at first glance it looks similar to the previously shown scattering in Voigt configuration the underlying processes are different. The exciting laser was tuned to the $M=0$ resonance and Brillouin scattering was observed via STA phonons from the $M=0$ to the $M=-1$ orthoexciton. For considering exclu-

sively STA interband scattering the same argument holds as in the case of Voigt configuration (see Table I) thus justifying the use of the selection rules. Again, LA interband scattering takes place within the $M=-1$ orthoexciton. The power dependence of the Brillouin scattering processes presented in the inset of Fig. 5 shows a more pronounced rise and saturation than in the measurements in Voigt configuration and spans over three orders of magnitude.

We observed stimulated Brillouin scattering in other crystallographic directions like for example $\mathbf{k}\|[112]$. The strength of the Brillouin scattering signal, however, varies from sample to sample which does not allow to compare absolute scattering intensities.

By tuning the laser through the orthoexciton resonance one observes a strong resonance dependence as presented in Fig. 6 for $\mathbf{k}\|[1\bar{1}0]$ and $B=4$ T in Voigt configuration. Shown are the stimulated Brillouin scattering intensities relative to the Raman transition whose resonance dependence follows the absorption. While approaching the resonance from lower energies, the stimulated Brillouin scattering intensity drops suddenly, particularly for the case of TA and subsequent LA scattering. Tuning the laser to higher energies, the scattering intensities increase slowly again. Due to this strong asymmetric resonance dependence the highest Brillouin scattering intensities are observed by tuning the laser slightly off-resonant. The origin of this asymmetric resonance dependence is not known up to now.

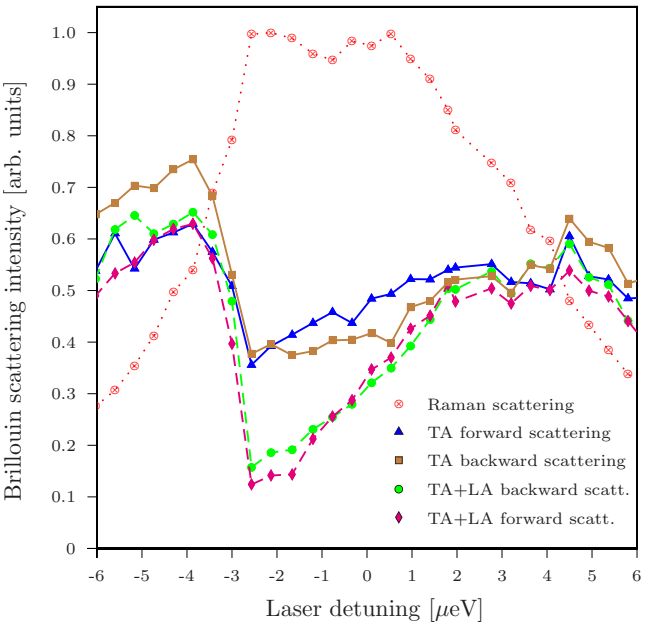

FIG. 6. (Color online) Resonance dependence of the Brillouin scattering lines as derived from the Γ_5^- phonon assisted luminescence at $B=4$ T in Voigt configuration.

V. CONCLUSIONS

In conclusion we have shown that orthoexcitons in Cu_2O are ideal candidates to investigate stimulated Brillouin scattering within exciton subbands. The intensity dependence of the Brillouin scattering lines exhibit a stimulation threshold for rather low excitation intensities. Beyond threshold each line splits into two lines. The emission becomes highly directional parallel and antiparallel to the exciting laser. The energetic positions of the stimulated Brillouin scattering lines in Voigt and Faraday configuration confirm our kinematic model and open the possibility to create states with arbitrary wavevector in the lowest two orthoexction states. A strong asymmetric resonance dependence makes the picture even richer.

ACKNOWLEDGMENTS

We acknowledge the support by the Deutsche Forschungsgemeinschaft (SFB "Starke Korrelationen im Strahlungsfeld" and Forschergruppe "Quantenoptik in Halbleitern").

*christian.sandfort@e2.physik.uni-dortmund.de

[1] R. G. Ulbrich and C. Weisbuch, Phys. Rev. Lett. **38**, 865 (1977).
[2] E. S. Koteles and G. Winterling, Phys. Rev. B **20**, 628 (1979).
[3] G. Baldassarri Höger von Högersthal, D. Fröhlich, M. Kulka, T. Auer, M. Bayer, and H. Stolz, Phys. Rev. B **73**, 035202 (2006).
[4] P. Y. Yu and Y. R. Shen, Phys. Rev. B **12**, 1377 (1975).
[5] A. Z. Genack, H. Z. Cummins, M. A. Washington, and A. Compaan, Phys. Rev. B **12**, 2478 (1975).
[6] G. Baldassarri Höger von Högersthal, G. Dasbach, D. Fröhlich, H. Stolz, and M. Bayer, J. Lumin. **112**, 25 (2005).
[7] G. Dasbach, D. Fröhlich, H. Stolz, R. Klieber, D. Suter, and M. Bayer, Phys. Rev. Lett. **91**, 107401 (2003); G. Dasbach, D. Fröhlich, R. Klieber, D. Suter, M. Bayer, and H. Stolz, Phys. Rev. B **70**, 121202 (2004).
[8] J. Brandt, D. Fröhlich, C. Sandfort, M. Bayer, H. Stolz, and N. Naka, Phys. Rev. Lett. **99**, 217403 (2007).
[9] J. Berger, Solid State Commun. **26**, 403 (1978).
[10] J. Hallberg and R. C. Hanson, Phys. Status Solidi. **42**, 305 (1970).
[11] J. I. Jang and J. P. Wolfe, Phys. Rev. B **73**, 075207 (2006).
[12] H_4 describes scattering via spin-orbit interaction which is much weaker (Ref. 11).
[13] C. Sandfort, J. Brandt, D. Fröhlich, M. Bayer, and H. Stolz, Phys. Rev. B **78**, 045201 (2008).
[14] M. Sparks, Phys. Rev. Lett. **32**, 450 (1974).
[15] Y. R. Shen and N. Bloembergen, Phys. Rev. **137**, A1787 (1965).